Hindawi
Complexity
Volume 2018, Article ID 1246381, 12 pages
https://doi.org/10.1155/2018/1246381

Research Article

Investigation of Speed Matching Affecting Contrarotating Fan's Performance Using Wireless Sensor Network including Big Data and Numerical Simulation

Hengxuan Luan,[1] **Liyuan Weng**,[2] **Ranhui Liu**,[1] **Yuanzhong Luan**,[2] **and Dongmin Li**[1,3]

[1]*Department of Mechanical & Electronic Engineering, Shandong University of Science and Technology, Taian, China*
[2]*College of Geomatics, Shandong University of Science and Technology, Qingdao, China*
[3]*State Key Laboratory of Fluid Power and Mechatronic System, Zhejiang University, Hangzhou, China*

Correspondence should be addressed to Hengxuan Luan; hengxuanluan@163.com

Received 11 June 2018; Accepted 2 August 2018; Published 10 September 2018

Academic Editor: Jaime Lloret

This paper describes the investigations performed to better understand two-stage rotor speed matching in a contrarotating fan. In addition, this study develops a comprehensive measuring and communication system for a contrarotating fan using ZigBee network. The investigation method is based on three-dimensional RANS simulations; the RANS equations are solved by the numerical method in conjunction with a SST turbulence model. A wireless measurement system using big data method is first designed, and then a comparison is done with experimental measurements to outline the capacity of the numerical method. The results show that when contrarotating fan worked under designed speed, performance of two-stages rotors could not be matched as the designed working condition was deviated. Rotor 1 had huge influences on flow rate characteristics of a contrarotating fan. Rotor 2 was influenced by flow rates significantly. Under large flow rate condition, the power capability of rotor 2 became very weak; under working small flow rate condition, overloading would take place to class II motor. In order to solve the performance mismatch between two stages of CRF under nondesigned working conditions, under small flow rate condition, the priority shall be given to increase of the speed of rotor 1, while the speed of rotor 2 shall be reduced appropriately; under large flow rate condition, the speed of rotor 1 shall be reduced and the speed of rotor 2 shall be increased at the same time.

1. Introduction

Development of high-performance turbomachinery is always an important orientation in the field of aeroengines. Thanks to unique advantages in structural and aerodynamic aspects, the contrarotating fan (CRF) technology is deemed as an important technology which can break through development limits in traditional rotor-stator blade row compressors and has drawn close attention from lots of scholars at present [1–3]. Basic ideas of the contrarotating fan technology are as follows: the stator component is canceled and the contrarotation of rotor is used to increase the power capability. In this way, the power capability of a fan/compressor can be increased effectively, and the original weight of it can be reduced greatly. The contrarotating fan technology is adopted in contrarotating fan/compressor [4], wherein the contrarotating impeller stage is a core component. Performance of the whole machine depends on performance of rotors at different stages.

Pundhir and Sharma and Sharma et al. [5, 6] conducted a comprehensive experimental research on a contrarotating axial compressor stage earlier, wherein the influence of factors such as speed ratio of the two rotors, rotor stagger, pitch-chord ratio, and axial spacing between the rotors was examined. The research results indicated that the performance of a contrarotating stage is affected by all these factors. Within the framework of the EU-funded project VITAL, SNECMA [7, 8] developed a contrarotating low-speed fan, wherein the final design goal was to achieve high efficiency and adequate acoustic performances for the given cycle

parameters. Mao and Liu and Mao et al. [9, 10] used numerical simulation methods to study the internal unsteady flow field of a contrarotating axial compressor in detail, wherein the unsteady effects of rotor-rotor interaction process and the unsteady behavior of tip flow were involved. To obtain a deeper insight into the flow physics in CRF, a large amount of work was conducted on the effects of some major factors [11–14]. A lot of useful results were obtained.

Due to the different ways of aerodynamic layout of a conventional fan/compressor, CRF's two-stage rotors on different shafts have problems in speed matching, which have attracted the attention of scholars. For CRF's two-stage rotor load distribution, designers generally believe that higher efficiency can be achieved with equal pressure rise distribution. However, in the actual work of CRF, the rear-stage rotor motor burnt out by accident [15]. Experimental studies showed that variable speed matching can improve the work stability [16]. Mistry and Pradeep [17, 18], through experiments and numerical simulations, reported a study of speed ratio on the performance of a contrarotating fan stage. Results showed that with increasing the speed ratio, the strong suction generated by the second rotor improves the stage pressure rise. Sun et al. [19] pointed out that with differential speed operation of two rotors, the CRF can work in the high-efficiency operating range.

Internet, big data, cloud computation, and Internet of Things are four promising emerging industries. Currently, wireless sensor networks and big data technologies are hot research areas in the information industry. Wireless sensor network technology has comprehensive processing capabilities such as sensing, data processing, storage, and wireless communication and has network deployment performance such as self-organization and self-healing. The wireless sensor networks in the Internet of Things era integrate multifunction sensors and actuators. The application of wireless sensor network technology has penetrated into various fields, including environmental monitoring [20], ocean exploration [21], intelligent transportation [22], and industrial safety production [23]. In aerodynamic experiments of fans, wired sensors are often used for data measurement. There are various types and huge numbers of monitored parameters, so it is complicated to install sensors and arrange signal lines, and mistakes can often be made. At industrial sites, application of the wired sensor monitoring will be more complicated and inconvenient. ZigBee is a close-range wireless communication protocol standard and is mainly applied in a wireless sensor network [24]. With the wireless sensor network, the complicated wiring link can be omitted, which can bring down the cost [25]. Jensen [26] emphasized the necessity of investing in WSNs' performance, based on model analysis and validation, before handling more critical functions. The British Petroleum Company applied the wireless sensor network technology to conduct vibration detection diagnosis of rotating machinery on a cruise ship and verified safety of the wireless sensor network in severe environments as well as accuracy and reliability of data transmission [27].

This paper proposes to design an axial fan monitoring system based on wireless sensor network and big data technology; by adjusting the rotor speed reasonably, the fan can operate safely and efficiently. The paper improves an aerodynamic experimental system of a fan at first and designs a system for wireless measurement of fan aerodynamic parameters based on the ZigBee technology. Then, through theoretical and numerical simulation and experiments, the paper analyzes operation characteristics of two-stage rotors of CRF and explains the performance mismatch between two-stage rotors under different working conditions. Furthermore, the paper makes a detailed research on performance parameters and flow characteristics of CRF under the variable speed matching and discusses a method which can optimize two-stage performance match under all the working conditions so as to realize safer and more efficient running of CRF in practical work.

Figure 1: The view of the contrarotating axial fan.

Table 1: Design parameters of the contrarotating axial fan.

Design parameter	Design speed (rpm)	Chord (tip/mid/hub) (mm)	Tip clearance (mm)
Rotor 1	−980	195.1/210.1/223.5	5
Rotor 2	980	194.8/209.7/222.6	5

2. Wireless Sensor Networks for Aerodynamic Experiment Based on ZigBee

The current investigation was performed on a contrarotating axial flow fan. Figure 1 shows the picture of the CRF (model: FBCDZ-number 20). Used for aerodynamic design, rotor blades of the front and rear rows are opposite in the direction of rotation. Stator blades are not applied to the aerodynamic design. The number of blades for the front rotor (rotor 1) and the rear rotor (rotor 2) was 19 and 17, respectively. The design volume flow of the fan was 64 m^3/s, and the outer diameter was 2000 mm. The other main design parameters of the CRF were shown in Table 1.

At present, high-precision sensors are installed in most fan experiment tables and conduct power supply and data transmission in a wired mode. Wired measurement is disadvantaged in high wiring complexity and inconvenience of installation and maintenance. Especially for turbomachinery with high-speed rotation, the conciseness of experimental rigs or monitoring systems shall be enhanced. The paper puts forward a wireless measurement system of fan aerodynamic parameters based on the ZigBee technology so as to avoid a lot of inconvenient aspects of the wired mode and enhance flexibility of the measurement system.

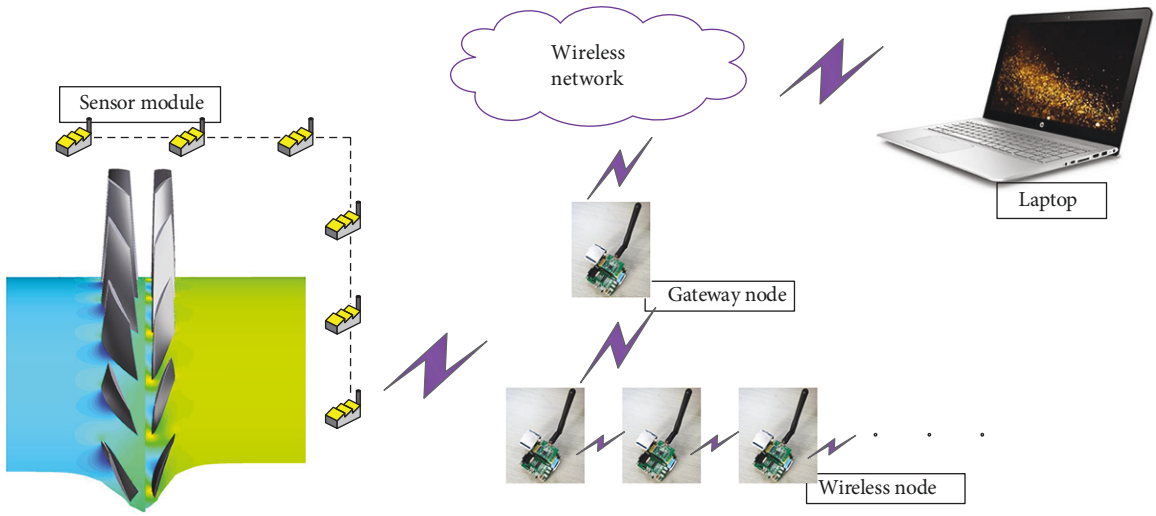

Figure 2: Applicable ZigBee nodes for contrarotating axial fan.

Compared to some short-range wireless communication protocols, such as Bluetooth, infrared, and Wi-Fi, ZigBee is a new type of wireless transmission protocol. ZigBee is a standard for low-rate, low-cost, and low-power applications. Due to its large coverage area and flexible network, ZigBee can meet the needs of industrial production field operations.

The overall design of the system includes a sensor module, a wireless sensor network, and a central computer. The overall design of the system is shown in Figure 2. The sensor module is composed of sensors, power, and ZigBee chips which integrates signal receiving and dispatching. It is mainly used to collect instant experimental data. The sensor module comprises an aerodynamic pressure sensor module, an aerodynamic load module, a temperature sensor module, a torque sensor module, and so on. The wireless sensor network is composed of gateway modes and different wireless nodes, wherein both parts conduct mutual communication based on the ZigBee technology. Each ZigBee node chip is equipped with the self-networking function. Different nodes can communicate with each other and realize network automatically. In the end, the data will be summarized to a ZigBee router which is set in the network. The ZigBee router and the central computer conduct serial port communication. With the central computer, experimenters can observe and record the measured instant aerodynamic parameters. In addition, due to the special environment of production site, the temperature states of nodes need to be considered. The temperature sensor can monitor the temperature of nodes in real time, and when the temperature of node is found to be too high, the buzzer will be used for alarming.

The signal receiving-dispatching CC2530 is used at the ZigBee node, wherein 8051CPU and the 265kB programmable flash memory are integrated inside. The CC2530 provides 101 dB of link quality, strong anti-interference, and high receiver sensitivity. It has multiple flash capacities, power modes, and peripherals. In addition to high-performance CPU, CC2530 also has excellent signal transceiver. The ZigBee router is composed of the ZigBee chip CC2530 and the hybrid signal processor MSP430G2553, wherein serial communication is used between MSP430G2553 and CC2530.

The aerodynamic pressure sensor module is composed of a ZigBee chip CC2530 and an aerodynamic pressure sensor. The hardware connecting mode of the aerodynamic pressure sensor module is shown in Figure 3. The MAS6512 chip is used. The I2C bus serial interface transmission mode is used for CC2530. The torque rotation speed sensor module is composed of the ZigBee chip CC2530 and a torque rotation speed sensor. The torque rotation speed sensor is used to output voltage-type frequency signals. After recognition by CC2530, they are transformed into corresponding digital signals.

The ZigBee router can receive and store ZigBee node data. According to serial communication parameters and the multiterminal communication self-networking protocol, the data can be transmitted to the central computer. The central computer continuously receives a large amount of data from the sensor nodes, which is the big data flow. The center computer mainly completes the analysis of aerodynamic data, adopts a program with the capabilities of rigorous data interpolation and mathematical fitting model, and can realize the aggregation and processing of big data.

3. Computational Procedures

CFX is used to solve the three-dimensional compressible Reynolds-averaged Navier-Stokes equations. The finite volume method is employed as the numerical method. The turbulence model of shear stress transport model [28] is applied, referred to as SST model, which is combined with advantages of k-ω turbulence model in terms of simulating the near-wall boundary layer and characteristics of k-ε turbulence model concerning small dependence towards far-field boundary conditions [29].

A composite grid system with structured grids was used to simulate the flow field accurately, with the total number of 2.1 million grids, as shown in Figure 4. The computing

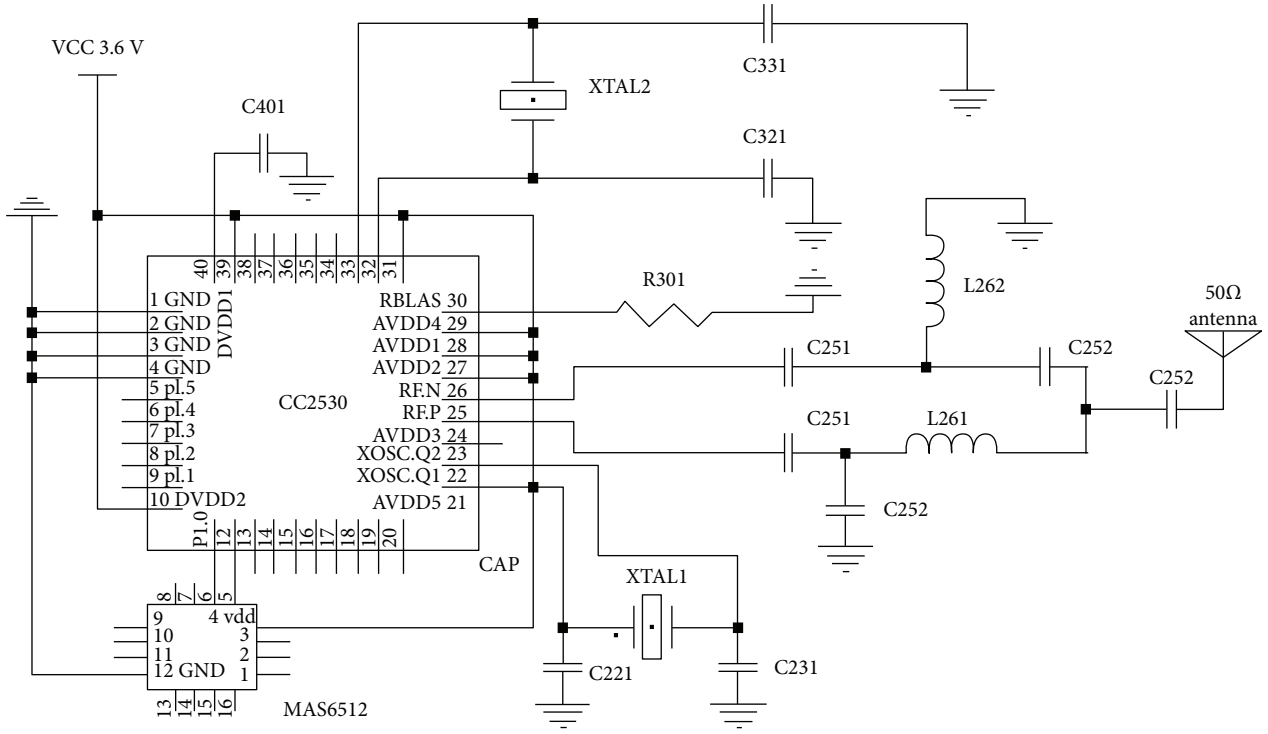

Figure 3: Pneumatic pressure sensor module.

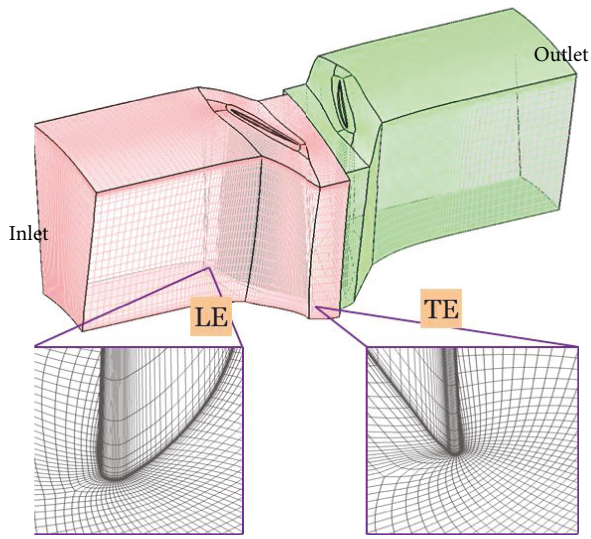

Figure 4: The computational mesh of the two rotors.

meshes are divided into domains of rotor 1 and rotor 2. The numbers of streamwise, spanwise, and pitchwise grid nodes of both rotor 1 and rotor 2 are $123 \times 85 \times 91$. To improve the quality of grids, O-block grid is applied on the plane area of blades, H-block grid is employed by the inlet and outlet and mainstream area, and butterfly grid topology is used in the clearance region. The first layer of mesh wall thickness of 0.003 mm gives $y+ < 2$ at the walls, thus meeting the requirements of turbulence model.

In order to verify the grid independence, 1.2 million grids are taken as the starting point, and 5 computations with different grid nodes are carried out from 0.8 million, 1.3 million, 1.7 million, 2.1 million, and 2.9 million, respectively. The distribution densities of the 5 different grid nodes are similar, which are mainly used for encryption. As indicated from the calculation, fan performance parameters are no longer sensitive to grid nodes when the number of nodes is more than 2.1 million. Therefore, 2.1 million grid nodes are applied for the calculation in the paper under comprehensive consideration of computational accuracy and time.

No-slip and adiabatic conditions are applied to all wall surfaces; the total temperature and total pressure of standard atmosphere as well as axial inflow are specified as the inlet boundary condition, while the static pressure is specified at the outlet assuming radial equilibrium. The stage method [30] is used to process the interface.

Thanks to continuous perfection of turbulence computation, various types of flowing can be simulated by numerical computation more accurately. However, certain errors and uncertain factors exist in numerical simulation. Till now, there is no numerical method that can accurately solve various types of flowing. Hence, before qualitative or quantitative analysis with numerical simulation, accuracy of the numerical simulation method shall be verified at first. Figure 5 gives parameters including total pressure and efficiency measured by CRF in experiments under the rated speed and also gives numerical simulation results under the same conditions. The paper mainly focuses on performance of variable speed matching of CRF. Hence, in the experiment, the flow rate was not reduced to the complete stall. Results in the diagram indicate that experimental data and numerical simulation conform with each other within the whole working scope, presenting basically the consistent changing trends. This

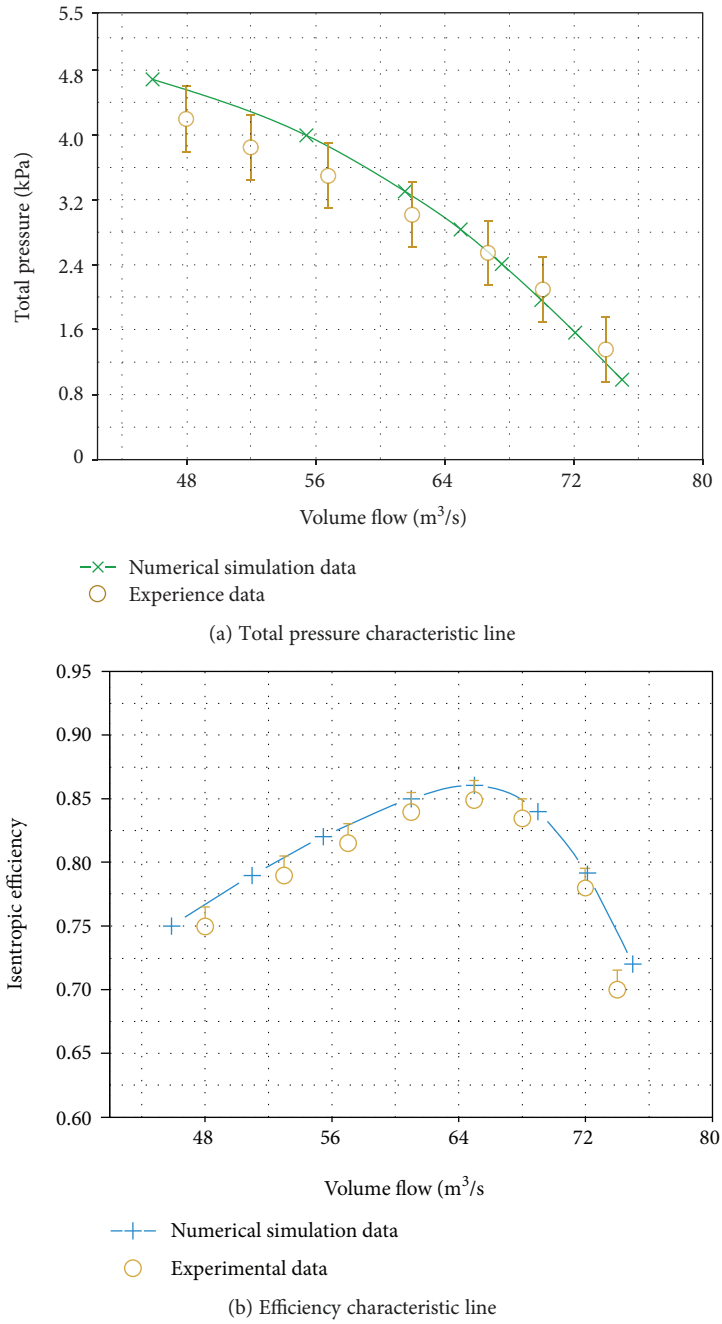

Figure 5: Characteristic lines of the contrarotating fan under design conditions.

result implies that the numerical simulation method used in the paper is reliable enough.

4. Aerodynamic Characteristics of Contrarotating Rotors at Base Speed

There is no guide blade at the entrance and exit of the CRF. The designed working condition was assumed as follows: axial gas entrance and axial gas exiting. On this basis, a speed triangle of the two-stage impeller was established, as shown in Figure 6. As for rotor 1, c_{11} and c_{12} denote absolute speeds of airflows at the entrance and exit of the rotor blade; w_{11} and w_{12} denote relative speeds of airflows at the entrance and exit of the rotor; β_{12} and α_{12} denote the relative speed of airflows at the exit and the airflow angle of absolute speed; u denotes the circular speed; and $\triangle c_{1u}$ denotes the circling speed at the airflow exit. As for rotor 2, the first footer 1 is changed to 2, while the meaning is not changed.

According to the Euler equation, the theoretical total pressure formula of the fan stage is as follows:

$$p = \rho u \Delta c_{1u}. \quad (1)$$

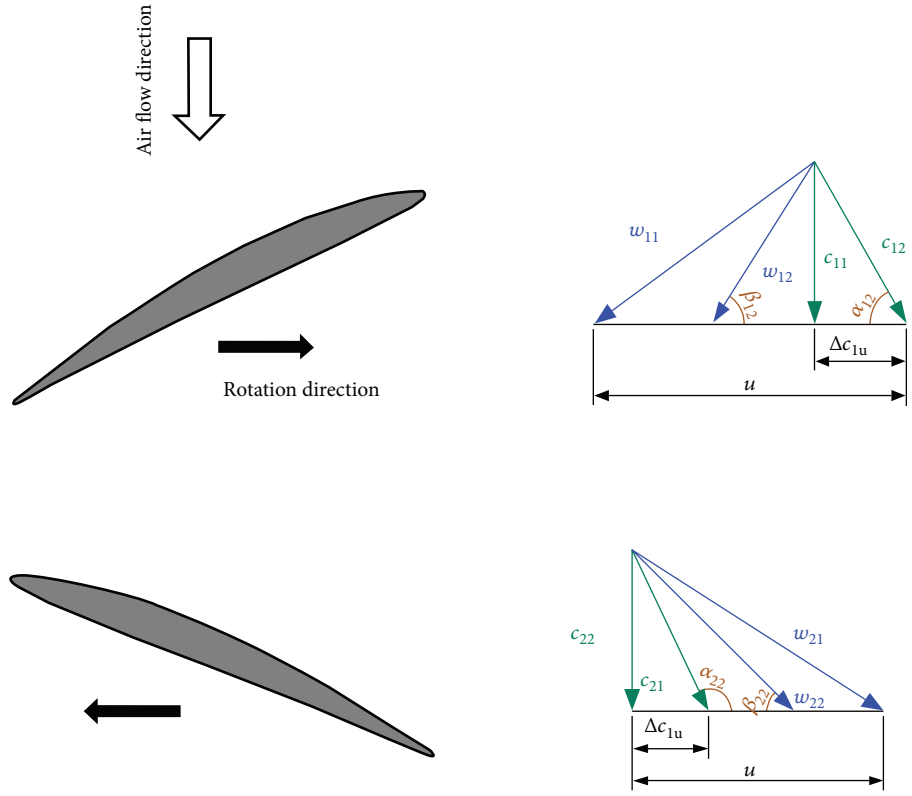

Figure 6: Velocity triangles for the contrarotating fan.

In the aerodynamic design of a conventional CRF, the first-stage and second-stage impellers are driven by the motors with the same power. The blades of the two stages have the same load, namely, $p_1 = p_2$. However, loads of two-stage rotors are the same only when the working flow rate is equal to the designed flow rate.

According to the speed triangle in Figure 6, the total pressure expression of the impeller of rotor 1 can be deduced as follows:

$$p_1 = \rho u \Delta c_{1u} = \rho u (u - c_z \cot \beta_{12}) = \rho u^2 \left(1 - \frac{\cot \beta_{12}}{uA} Q\right), \tag{2}$$

where c_z denotes the axial speed component of airflows, Q denotes the volume flow rate, and A denotes the flow area of the airflow.

Similarly, as for rotor 2,

$$\begin{aligned} p_2 &= \rho u \Delta c_{2u} = \rho u (c_z \cot \alpha_{12} - c_z \cot \beta_2 + u) \\ &= \rho u^2 \left(1 - \frac{\cot \beta_{12}}{uA} Q\right) + \rho u^2 \left(1 - \frac{\cot \beta_{22}}{uA} Q\right) \\ &= p_1 + \rho u^2 \left(1 - \frac{\cot \beta_{22}}{uA} Q\right). \end{aligned} \tag{3}$$

According to formulas (2) and (3), we can find that when the working flow rate is equal to the designed flow rate, namely, $Q = uA/cot\beta_{22}$, the theoretical total pressures of two stages were equal. If Q is smaller than the designed flow rate, the total pressure rise p_2 of the rotor 2 is larger than the total pressure rise p_1 of the rotor 1. If Q is larger than the designed flow rate, p_2 will be smaller than p_1.

Theoretical powers of rotor 1 and rotor 2 are as follows:

$$\begin{aligned} N_1 &= p_1 Q, \\ N_2 &= p_2 Q. \end{aligned} \tag{4}$$

Formula (4) is substituted into formulas (1) and (2), so

$$N_1 = \rho u^2 \left(Q - \frac{\cot \beta_{12}}{uA} Q^2\right), \tag{5}$$

$$N_2 = p_1 Q + \rho u^2 \left(Q - \frac{\cot \beta_{22}}{uA} Q^2\right). \tag{6}$$

According to formula (5), when $1 - (\cot \beta_{22}/uA)Q = 0$ is satisfied, namely, Q is the designed flow rate, $N_2 = N_1$ will be satisfied. When Q is smaller than the designed flow rate, $N_2 > N_1$. When Q is larger than the designed flow rate, $N_2 < N_1$. In addition, according to formulas of theoretical total pressure and theoretical power of two stages of rotors, we can find that obvious differences exist in total pressures and powers of two-stage rotors of CRF under the varying conditions.

According to the unitary theoretical model, we can obtain general rules of total pressure characteristics and power characteristics of the two-stage rotors. In order to know

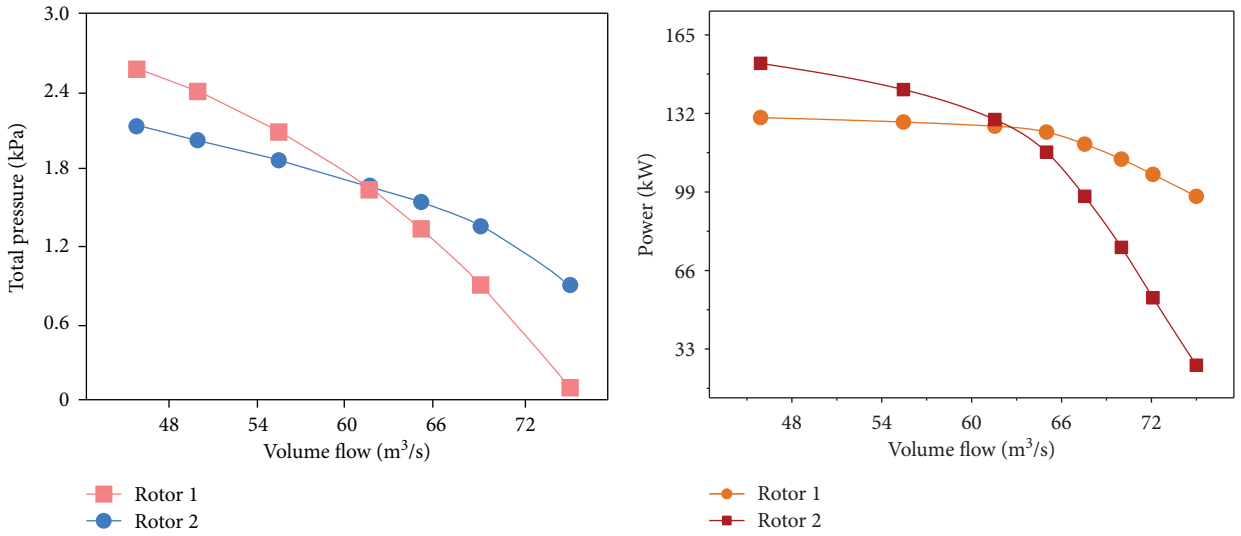

(a) Characteristic line of total pressure

(b) Characteristic line of shaft power

Figure 7: Total pressure and shaft power characteristic lines of two-stage rotors under design condition.

aerodynamic parameter characteristics of two-stage rotors more directly, Figure 7 gives total pressure and shaft power curve diagrams of two-stage impellers under the designed rotation speed. It is shown in the figure that, within the whole flow rate scope, the total pressure changing amplitude of rotor 1 was smaller than that of rotor 2. When the flow rate of CRF was smaller than the designed flow rate, the total pressure rise of rotor 2 was larger than that of rotor 1. When the flow rate was larger than the designed flow rate, the total pressure of rotor 2 was lower than that of rotor 1. With continuous increase of the flow rate, the power capability of rotor 2 became very weak. Within the whole flow rate scope, the shaft power changing degree of rotor 1 was relatively small. Hence, the class I motor can keep a steady state. However, the shaft power of rotor 2 changed a lot with the flow rate change. When CRF was operated under a small flow rate working condition, the shaft power of rotor 2 increased, while the class II motor might be burnt due to overloading. Under the large flow rate working condition, the shaft power of rotor 2 decreased sharply. The above phenomena are the same with theoretical analysis results. Hence, when CRF was deviated from the designed working condition, serious mismatch took place to two stages of rotors.

Figure 8 gives a static pressure contour of the S1 face along the flow direction as well as streamlines near the blades. Impeller rotation acted power on gas, so gas static pressure gradually increased along the flow direction and reached the maximum value in the downstream of rotor 2. Under the influence of the boundary layer and the trailing edge thickness, there are high turbulence and high energy dissipation wake at the trailing edge of blade. The wake is affected by pressure gradients and velocity gradients in the flow passage and is cut by rotor 2 during the downward transport. Impacted by mainstream and upstream wakes, an area with high static pressure values existed on the leading edge of the rotor 2 blade. According to the flow line diagram, we can find that the angle of attack at the 50% of blade spreading height was rational, flowing was stable in CRF, and flow separation did not exist.

5. Aerodynamic Characteristics of Contrarotating Rotors under Variable Speed

According to the analysis in Section 4, we can find that CRF had good aerodynamic performance under the designed working condition, while two-stage motors could run stably. However, when the designed working condition was deviated, huge differences existed in total pressure and power characteristics of the two-stage rotors. Specifically, under working conditions with small flow rates, loads of the rotor 2 were large, which might lead to overloading of the class II motor. Under working conditions with large flow rates, the whole machine efficiency of CRF decreased very quickly, while the power capability and power of rotor 2 decreased sharply. Aiming at the above problems, this section carries out research on variable speed matching of two-stage rotors.

Designed speed of two-stage rotors of CRF is 980 rpm. In the paper, 980 rpm is taken as the standard. When the speed of a stage was kept unchanged, the speed of the other stage was adjusted to 0.6, 0.8, 1.2, and 1.4 times the designed speed. Table 2 shows a detailed proposal of variable speed matching.

Figure 9 shows the total pressure characteristic line of CRF under different speed matching. It is shown in the diagram that, according to comparison between the CRF with different speed matching and the conventional CRF, their characteristic lines basically have the consistent trends. Based on the designed speed, with the decrease in speeds of rotor 1 or rotor 2, the total pressure rise of the whole CRF gradually decreased; with the increase of speed of rotor 1 or rotor 2, the total pressure rise of the whole CRF gradually increased.

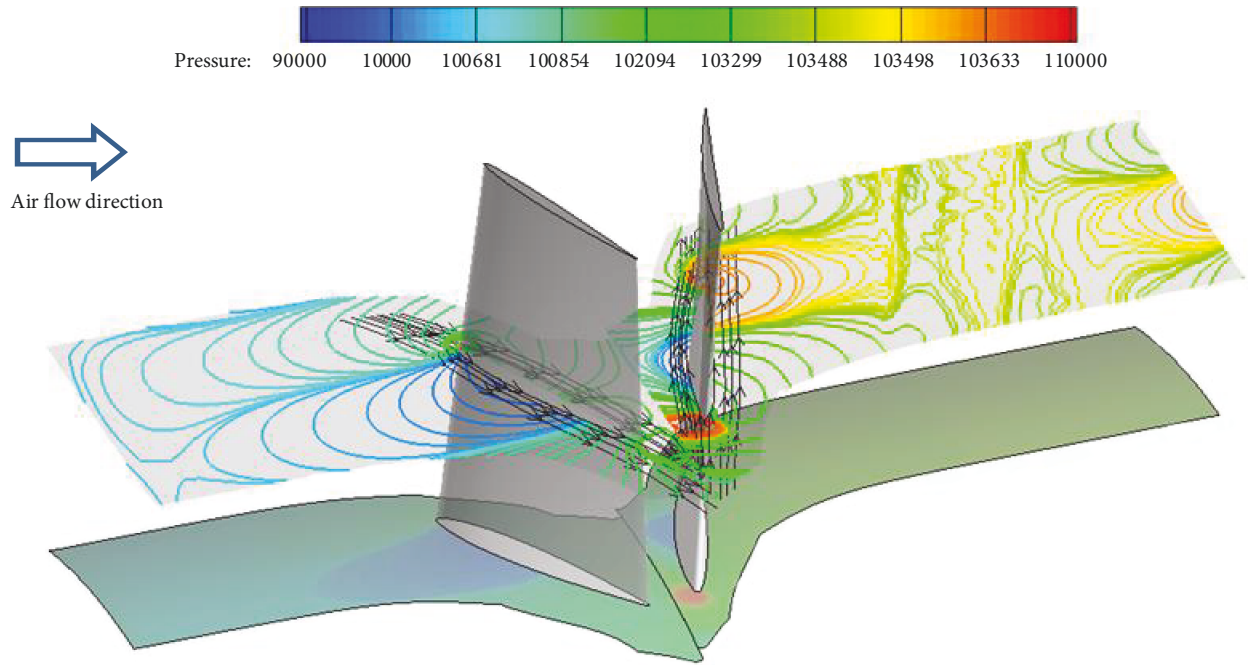

Figure 8: The static pressure contour of CRF under design condition.

Table 2: The scheme of variable rotating speed matching.

Percentage change in speed	Variable rotor 1 speed		Variable rotor 2 speed	
	Rotor 1	Rotor 2	Rotor 1	Rotor 2
−40%	588	980	980	588
−20%	784	980	980	784
0	980	980	980	980
20%	1176	980	980	1176
40%	1372	980	980	7372

When the speed of rotor 2 was fixed at the designed value 980 rpm, after changing of speed of rotor 1, obvious deviation would appear in flow rates of the stall boundary of CRF. However, when the speed of rotor 1 was fixed at the designed speed, changes in the speed of rotor 2 did not have huge influences on flow rates of the stall boundary of CRF. Hence, rotor 1 had huge influences on flow rate characteristics of CRF. This is because in the CRF, the flow field condition of rotor 2 is more dependent on rotor 1, because there was no stator between the two-stage rotors to organize the airflow. Rotor 2 not only played the role of pressure but also converted the work of rotor1 on the airflow into pressure potential energy, so rotor 1 had a great influence on the aerodynamic characteristics of the CRF. Through comparison of CRF characteristic lines under the same speed difference, we can find that when the percentage change in speed was larger than 0, the flow rate scope of the variable speed of rotor 1 was obviously narrower than that of the variable speed of rotor 2. The difference is that, when the percentage change in speed is smaller than 0, with the decrease in speeds of rotor 2, the flow rate scope of the whole CRF turned narrower obviously. Changing of speed of rotor 1 did not have huge influences on the flow rate scope of CRF.

In order to know aerodynamic characteristics of different rotors of CRF, Figure 10 gives the total pressure characteristic lines of two-stage rotors under variable speed. It is shown in the diagram that, when the speed of rotor 2 was kept unchanged, with the increase of speeds of rotor 1, the total pressure of rotor 1 increased significantly and the total pressure of rotor 2 decreased. When the speed of rotor 1 was kept changed, with the increase of speeds of rotor 2, the total pressure of rotor 2 gradually increased, while the total pressure of rotor 1 decreased. In addition, when the percentage change in speed was larger than 0, the changing in speeds of rotor 1 had more obvious influences on total pressure characteristics of two-stage rotors.

Figure 11 gives the shaft power characteristic lines of two-stage rotors under variable speed. It is shown that, when the speed of rotor 2 was kept unchanged, with the increase of speeds of rotor 1, the shaft power of rotor 1 increased significantly and the shaft power of rotor 2 gradually decreased, while the changing degree of shaft power of rotor 1 was obviously larger than that of rotor 2. When the speed of rotor 1 was kept unchanged, with the increase of speeds of rotor 2, the shaft power of rotor 2 increased significantly, while shaft powers of rotor 1 gradually decreased. It is similar with the total pressure characteristics. When the percentage change in speed was larger than 0, the speed change in rotor 1 had huge influences on power characteristics of two-stage rotors.

In order to solve the problem of serious mismatch between two-stage rotors, which appear when the CRF is deviated from the rated working condition, based on the above analysis results, we find that it is necessary to increase the speed of rotor 1 properly and reduce the speed of rotor 2

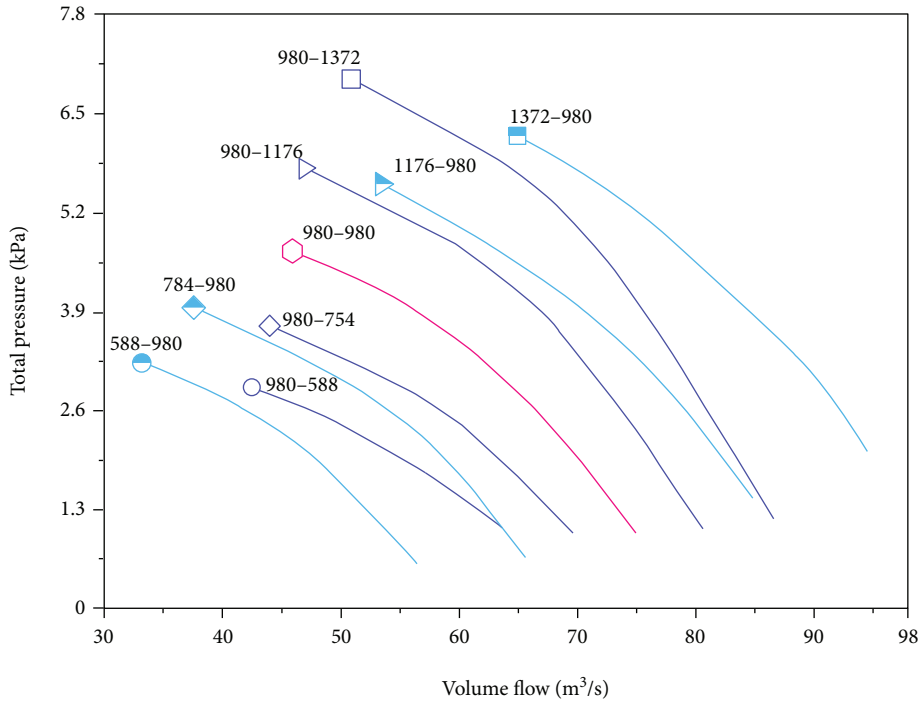

Figure 9: Total pressure curve of CRF at variable speed matching.

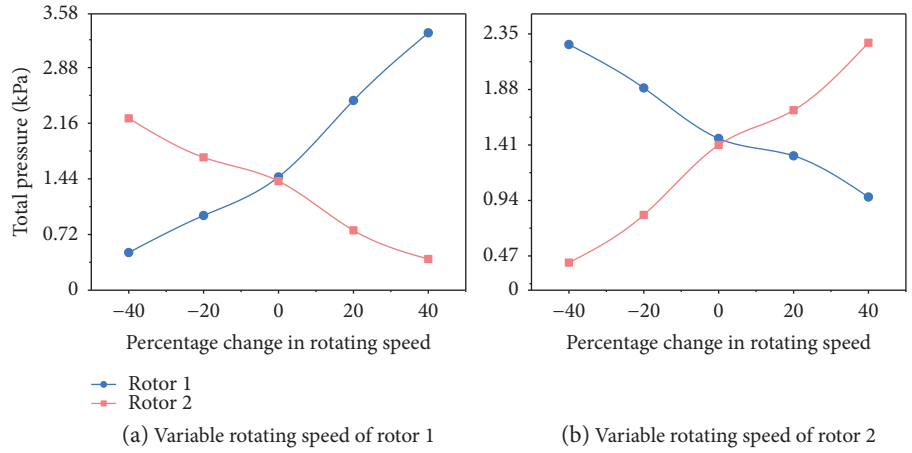

(a) Variable rotating speed of rotor 1 (b) Variable rotating speed of rotor 2

Figure 10: Total pressure characteristic lines of two-stage rotors under variable rotating speed.

properly under small flow rate condition. Under large flow rate condition, the speed of rotor 1 shall be reduced properly, while the speed of rotor 2 shall be increased properly. Through rational distribution of loads and powers of two-stage rotors, the CRF can work more safely and efficiently under different working conditions.

Figure 12 gives the streamline diagram of CRF with speed variation under small flow rates. It is shown that, under small flow rate condition, the airflow attack angles of rotor 1 were large, while the horseshoe vortex branch had a separated structure on the suction surface. Obvious flow separation existed on the suction surface of rotor 2. Low-energy fluids flowed out to the tailing edge with the radial fluid channeling under comprehensive effects of centrifugal force and blade force. When the speed of rotor 2 was kept unchanged, with the increase of speed of rotor 1, airflow attack angles of the two stages were improved effectively, while flow separation on the suction surface of rotor 2 was weakened. When the speed of rotor 1 was kept changed, with the decrease of speed of rotor 2, airflow separation near the suction surface of rotor 1 was more obvious, wherein the separation line was moved to the leading edge and the separation area was enlarged. Meanwhile, the separation area generated by rotor 2 in the suction surface corner area was enlarged. Hence, when the CRF works under small flow rates, the speed of rotor 1 shall be increased.

Figure 13 gives the streamline diagram of CRF with speed variation under large flow rates. It is shown that, under different variant speed matching, rotor 1 and rotor 2 stayed at

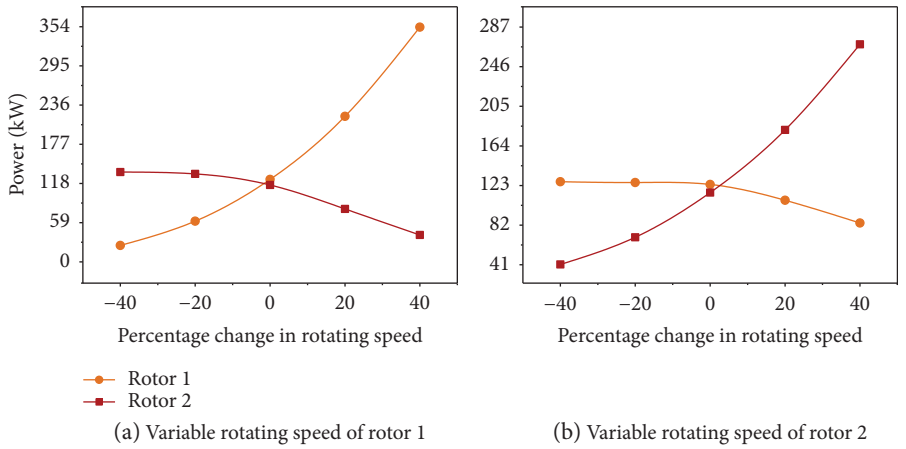

(a) Variable rotating speed of rotor 1 (b) Variable rotating speed of rotor 2

Figure 11: Shaft power characteristic lines of two-stage rotors under variable rotating speed.

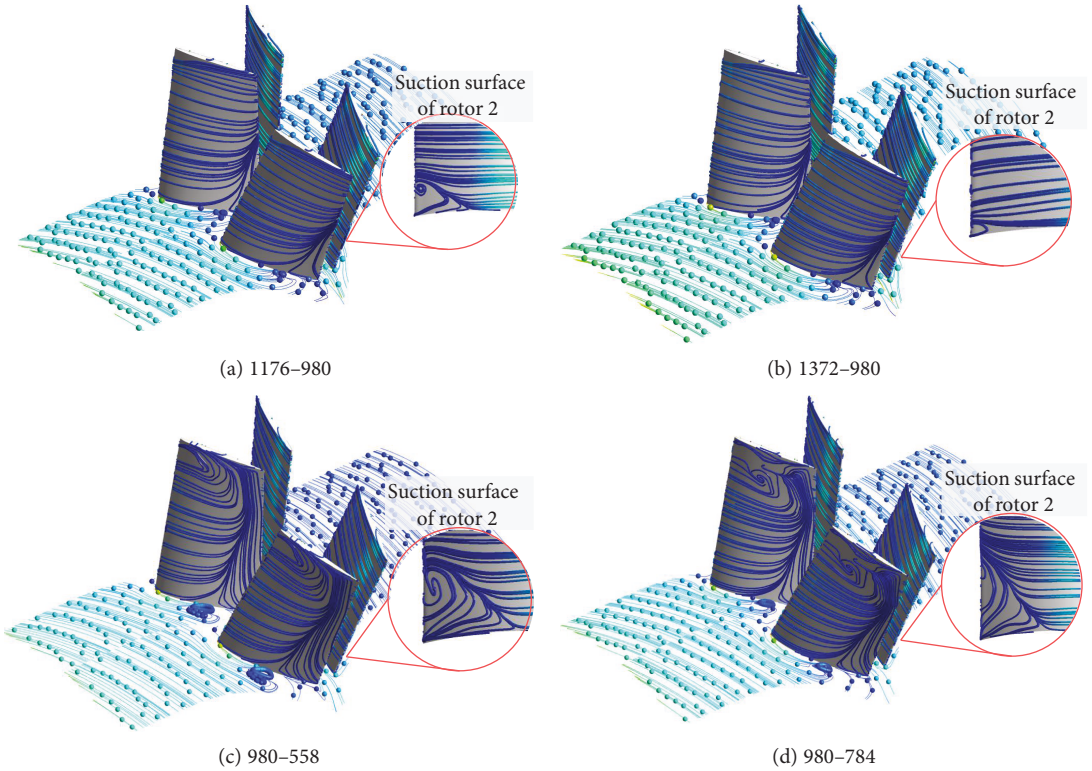

(a) 1176–980 (b) 1372–980

(c) 980–558 (d) 980–784

Figure 12: Streamline diagram of CRF with rotating speed variation under small flow conditions.

states with obvious negative attack angles, while corner separation on the suction surface basically disappeared. Separation did not take place in the whole flow passage, while the organization of internal flow field was good. Hence, when CRF works under large flow rates, these two methods of variable speed matching can be taken into account.

6. Conclusions

(1) This paper designs a wireless measurement system of fan's aerodynamic parameters, based on ZigBee technology and big data method. As for data transmission, the traditional wired mode is replaced by the wireless mode.

(2) When two-stage rotors of CRF worked under the equal speed, performance of two-stage rotors could not be matched as the designed working condition was deviated. Rotor 2 was influenced by flow rates significantly. Under the large flow rate condition, the power capability of rotor 2 became very weak. Under the small flow rate condition, overloading would take place to class II motor. The class I motor could work stably within the whole scope of flow rates.

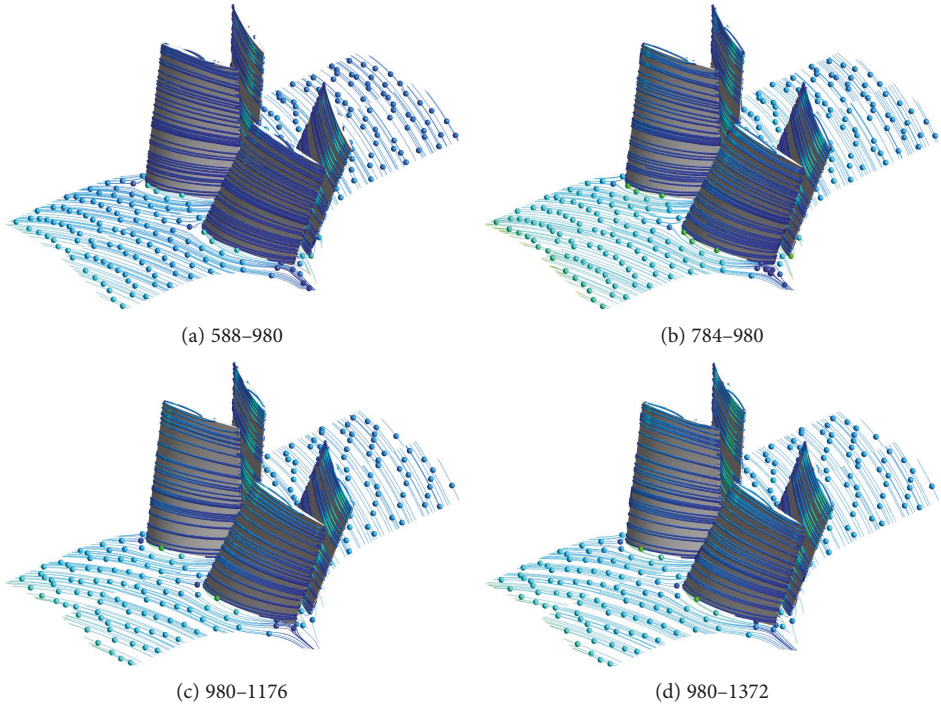

(a) 588–980 (b) 784–980

(c) 980–1176 (d) 980–1372

Figure 13: Streamline diagram of CRF with rotating speed variation under large flow conditions.

(3) Rotor 1 had huge influences on flow rate characteristics of CRF. During variable speed matching, rotor 1 had huge influences on flow rates of the stall boundary. Variable speed matching of two-stage rotors could influence the flow rate scope of CRF to a certain extent.

(4) When the speed of rotor 2 was kept unchanged, with the increase of speed of rotor 1, the total pressure and shaft power of rotor 1 increased significantly, while the total pressure of the shaft power of rotor 2 decreased. When the speed of rotor 1 was kept unchanged, with the increase of speeds of rotor 2, the total pressure and shaft power of rotor 2 gradually increased, while total pressure and shaft power of rotor 1 decreased.

(5) In order to solve the performance mismatch between two stages of CRF under nondesigned working conditions, different measures can be taken under small and large flow rates, respectively. Under working conditions with small flow rates, the priority shall be given to increase the speed of rotor 1, while the speed of rotor 2 shall be reduced appropriately; under working conditions with large flow rates, the speed of rotor 1 shall be reduced and the speed of rotor 2 shall be increased at the same time.

Data Availability

The data used to support the findings of this study are available from the corresponding author upon request.

Conflicts of Interest

The authors declare that there are not any conflicts of interest regarding the publication of this paper.

Acknowledgments

The authors would like to acknowledge the support of the Scientific Research Foundation of Shandong University of Science and Technology for Recruited Talents (Grant no. 2017RCJJ078), the support of the Key Research and Development Plan of Shandong Province (Grant no. 2017GSF220010), and the support of the Open Foundation of the State Key Laboratory of Fluid Power Transmission and Control (Grant no. GZKF-201614).

References

[1] C. Wang and L. Huang, "Passive noise reduction for a contra-rotating fan," *Journal of Turbomachinery*, vol. 137, no. 3, article 031007, 2015.

[2] M. Heinrich, C. Friebe, and R. Schwarze, "Experimental and numerical investigation of a gearless one-motor contra-rotating fan," *Proceedings of the Institution of Mechanical Engineers, Part A: Journal of Power and Energy*, vol. 230, no. 5, pp. 467–476, 2016.

[3] T. Shigemitsu, K. Tanaka, K. Hirosawa, and K. Miyazaki, "Internal flow condition between front and rear rotor of contra-rotating small-sized axial fan at low flow rate," *Open Journal of Fluid Dynamics*, vol. 7, no. 4, article 81518, 15 pages, 2017.

[4] J. Xu, C. Tan, H. Chen, Y. Zhu, and D. Zhang, "Influence of tip clearance on performance of a contra-rotating fan," *Journal of Thermal Science*, vol. 18, no. 3, pp. 207–214, 2009.

[5] D. S. Pundhir and P. B. Sharma, "A study of aerodynamic performance of a contra rotating axial compressor stage," *Defence Science Journal*, vol. 42, no. 3, pp. 191–199, 1992.

[6] P. B. Sharma, Y. P. Jain, and D. S. Pundhir, "A study of some factors affecting the performance of a contra-rotating axial compressor stage," *Proceedings of the Institution of Mechanical Engineers, Part A: Power and Process Engineering*, vol. 202, no. 1, pp. 15–21, 1988.

[7] J. Talbotec and M. Vernet, "Snecma counter rotating fan aerodynamic design logic & tests results," in *27th International Congress of Aeronautical Sciences*, pp. 19–24, Nice, France, 2010.

[8] T. Lengyel-Kampmann, A. Bischoff, R. Meyer, and E. Nicke, "Design of an economical counter rotating fan: comparison of the calculated and measured steady and unsteady results," in *ASME Turbo Expo 2012: Turbine Technical Conference and Exposition*, pp. 323–336, American Society of Mechanical Engineers, Copenhagen, Denmark, 2012.

[9] X. Mao and B. Liu, "Numerical investigation of the unsteady flow behaviors in a counter-rotating axial compressor," *Proceedings of the Institution of Mechanical Engineers, Part A: Journal of Power and Energy*, vol. 230, no. 3, pp. 289–301, 2016.

[10] X. Mao, B. Liu, and H. Zhao, "Numerical analysis of the circumferential grooves casing treatment in a counter-rotating axial flow compressor," *Applied Thermal Engineering*, vol. 130, pp. 29–39, 2018.

[11] H. Luan, L. Weng, Y. Luan, Y. Zhang, and P. Chen, "Numerical study on aerodynamic noise performances of axial spacing in a contra-rotating axial fan," *Journal of Vibroengineering*, vol. 18, no. 8, pp. 5605–5618, 2016.

[12] C. Wang, "Trailing edge perforation for interaction tonal noise reduction of a contra-rotating fan," *Journal of Vibration and Acoustics*, vol. 140, no. 2, article 021016, 2018.

[13] T. D. Toge and A. M. Pradeep, "Experimental investigation of stall inception of a low speed contra rotating axial flow fan under circumferential distorted flow condition," *Aerospace Science and Technology*, vol. 70, pp. 534–548, 2017.

[14] H. Luan, Q. Chen, L. Weng, Y. Luan, and P. Chen, "Effect of counter-rotating fan's speed matching on stall inception and characteristics of tip clearance flow," *Journal of Vibroengineering*, vol. 19, no. 6, pp. 4630–4643, 2017.

[15] J. Wen, Y. Tang, J. He, and H. He, "Numerical calculation and optimization of fluid flow field of external fan of high voltage asynchronous motors," *Electric Machines and Control*, vol. 17, pp. 79–85, 2013.

[16] Y.-Y. Chen, B. Liu, Y. Xuan, and X.-R. Xiang, "A study of speed ratio affecting the performance of a contra-rotating axial compressor," *Proceedings of the Institution of Mechanical Engineers, Part G: Journal of Aerospace Engineering*, vol. 222, no. 7, pp. 985–991, 2008.

[17] C. Mistry and A. Pradeep, "Effect of variation in axial spacing and rotor speed combinations on the performance of a high aspect ratio contra rotating axial fan stage," *Proceedings of the Institution of Mechanical Engineers, Part A: Journal of Power and Energy*, vol. 227, no. 2, pp. 138–146, 2013.

[18] C. Mistry and A. Pradeep, "Effect of speed ratio and axial spacing variations on the performance of a high aspect ratio, low speed contra-rotating fan," in *ASME Turbo Expo 2012: Turbine Technical Conference and Exposition*, pp. 63–71, American Society of Mechanical Engineers, Copenhagen, Denmark, 2012.

[19] X. Sun, D. Meng, B. Liu, and Q. Wang, "Numerical investigation of differential speed operation of two impellers of contra-rotating axial-flow fan," *Advances in Mechanical Engineering*, vol. 9, no. 10, Article ID 168781401772008, 2017.

[20] W. Wei, Z. Sun, H. Song, H. Wang, X. Fan, and X. Chen, "Energy balance-based steerable arguments coverage method in WSNs," *IEEE Access*, vol. 6, pp. 33766–33773, 2018.

[21] J. Wu, H. Hu, and M. Uysal, "High-rate distributed space-time-frequency coding for wireless cooperative networks," *IEEE Transactions on Wireless Communications*, vol. 10, no. 2, pp. 614–625, 2011.

[22] J. Li, S. He, Z. Ming, and S. Cai, "An intelligent wireless sensor networks system with multiple servers communication," *International Journal of Distributed Sensor Networks*, vol. 11, no. 8, Article ID 960173, 2015.

[23] J. Wu, Y. D. Zhang, M. G. Amin, and M. Uysal, "Multiple-relay selection in amplify-and-forward cooperative wireless networks with multiple source nodes," *EURASIP Journal on Wireless Communications and Networking*, vol. 2012, no. 1, 256 pages, 2012.

[24] J. Lee, Y. Su, and C. Shen, "A comparative study of wireless protocols: Bluetooth, UWB, Zig Bee, and Wi-Fi," in *IECON 2007 - 33rd Annual Conference of the IEEE Industrial Electronics Society*, pp. 46–51, Taipei, Taiwan, 2007.

[25] M. A. Moridi, M. Sharifzadeh, Y. Kawamura, and H. D. Jang, "Development of wireless sensor networks for underground communication and monitoring systems (the cases of underground mine environments)," *Tunnelling and Underground Space Technology*, vol. 73, pp. 127–138, 2018.

[26] K. Jensen, *Transactions on Petri Nets and Other Models of Concurrency VIII*, Springer, 2013.

[27] S. Fu and H. Song, "Design of mine ventilators monitoring system based on wireless sensor network," *Journal of Physics: Conference Series*, vol. 364, article 012011, 2012.

[28] F. R. Menter, "Two-equation eddy-viscosity turbulence models for engineering applications," *AIAA Journal*, vol. 32, no. 8, pp. 1598–1605, 1994.

[29] S. M. El-Behery and M. H. Hamed, "A comparative study of turbulence models performance for separating flow in a planar asymmetric diffuser," *Computers & Fluids*, vol. 44, no. 1, pp. 248–257, 2011.

[30] N. Gourdain, "Prediction of the unsteady turbulent flow in an axial compressor stage. Part 1: comparison of unsteady RANS and LES with experiments," *Computers & Fluids*, vol. 106, pp. 119–129, 2015.